Cite This: Anal. Chem. 2017, 89, 12587-12595

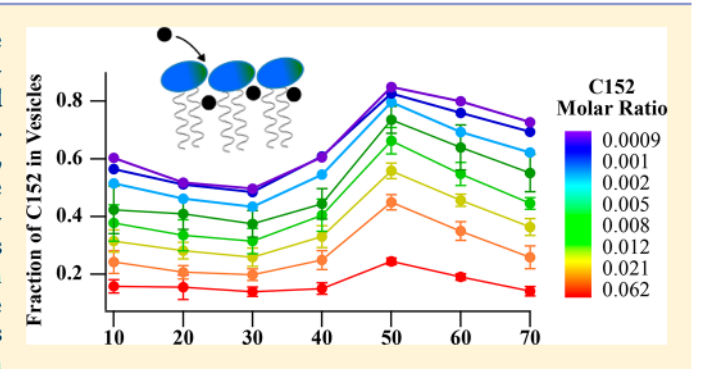
Quantifying Solute Partitioning in Phosphatidylcholine Membranes

Christine A. Gobrogge[†] and Robert A. Walker*,^{†,‡}

[†]Chemistry and Biochemistry Department, Montana State University, Bozeman, Montana 59717, United States

Supporting Information

ABSTRACT: Time-resolved fluorescence measurements were used to characterize and quantify solute partitioning into 1,2dipalmitoyl-sn-glycero-3-phosphocholine (DPPC) lipid vesicles as a function of solute concentration and temperature. The solutes, coumarin 152 (C152) and coumarin 461 (C461), both belong to a family of 7-aminocoumarin dyes that have distinctive fluorescence lifetimes in different solvation environments. The two solutes differ in the 4-position where C152 has a trifluoromethyl group in place of C461's -CH3 group. In vesicle containing solutions, multiexponential fluorescence decays imply separate solute populations in the aqueous buffer, solvated in the vesicle headgroup region and solvated in



the acyl chain bilayer interior, respectively. Fluorescence amplitudes, corrected for differences in radiative rates, are used to calculate absolute partition coefficients and average number of solutes per vesicle as a function of coumarin:lipid ratio and average number of solutes per vesicle. Results show that C152 has an ~10-fold greater affinity than C461 for lipid bilayers, despite both solutes having similar hydrophobicities as inferred from their log(P) values. Temperature-dependent partitioning data are used to calculate enthalpies and entropies of C152 partitioning as a function of concentration. These values are used to extrapolate to the infinitely dilute limit. Above and below the lipid gel-liquid crystalline temperature, partitioning is exothermic with negative changes in entropy. In the vicinity of the transition temperature, these quantities change sign with ΔH_{part} becoming endothermic (+70 kJ/mol) and entropically favored ($\Delta S_{part} = +240 \text{ J/(mol · K)}$).

C olute partitioning into lipid membranes underpins a host of biological phenomena ranging anesthetic action to pharmaceutical activity to bioaccumulation of pollutants. 1-3 For years, selective halogenation of solutes has been used to increase biological membrane binding and partitioning.4-6 A common practice to enhance passive diffusion of solutes into membranes is to replace hydrogens with a chlorine or trifluoromethyl moiety. Fluorinated drugs make up ~20% of all pharmaceuticals, up to ~30% of agrochemicals, and a quarter of all patents, and synthetic procedures in medicinal chemistry involve selective halogenation as a final step of drug synthesis.8 Despite the importance of halogens in modern pharmacology and ecology, however, relatively few models can predict quantitative, molecular-level details about solutemembrane interactions. The enhanced lipophilicity shown by halogenated solutes has been attributed to larger molecular volumes and increased cross-sectional areas, but these effects fail to account for specific, noncovalent forces that drive membrane partitioning.⁵ Furthermore, once a solute has partitioned into a membrane, empirically developed descriptions of biological activity cannot anticipate solute distributions across the heterogeneous membrane environment.

Along with solute structure, membrane packing strongly influences solute partitioning. Since membrane packing changes dramatically with temperature, solute/membrane partition coefficients have similarly been shown to have a strong temperature dependence. Below their melting temperature, phospholipid membranes exist in a highly ordered, rigid, gel state. Lower partition coefficients have been recorded when membranes are in this phase as compared to membranes in their fluid, liquid crystalline phase. Studies using a wide variety of solutes show that the partition coefficient reaches a maximum at the membrane melting temperature due to an increase in lateral density fluctuations. 9,10 A reduction in partition coefficients has been observed with beta blockers, dopamine, and local anesthetics at temperatures well above the membrane melting temperature. 11 The decrease in partitioning may be attributed to the increase in water solubility of hydrophobic molecules at higher temperatures or the conformational changes of lipid headgroups. 11,12

Many studies have quantitatively investigated how halogen identity and position changes a solute's membrane binding affinity. However, the techniques used in these reports do not directly nor quantitatively measure partitioning into the different heterogeneous microenvironments of membranes at different temperatures. Common techniques used to estimate partitioning in pharmacological development and in ecological assessments include computational simulations ^{13,14} and QSARs

September 27, 2017 Received: Accepted: October 20, 2017 Published: October 20, 2017



^{*}Montana Materials Science Program, Montana State University, Bozeman, Montana 59717, United States

(quantitative structure-activity relationships). 15-17 Air/water partitioning experiments are sometimes used to mimic partitioning at the membrane interface, but such experiments do not account for the small heterogeneous microenvironments present in membranes. Differences in lipid-water partitioning thermodynamics of promazine, perazine, and perphenazine (and their halogenated analogues) have been quantified using surface activity measurements. This study found that replacing a hydrogen by a chlorine and trifluoromethyl group increases the partitioning coefficient by factors of ~2 and ~9, respectively, while the replacement increases the free energy of partitioning by -1.3 and -4.5 kJ/mol, respectively. Results indicated that the increase in partitioning coefficient was dominated by the increase in solute hydrophobicity as opposed to the increase in molecular cross-sectional area.5 Missing from this study, however, was any sort of description about where these solutes partitioned within a lipid membrane itself.

Several other techniques have also been used to detect solute-membrane interactions, including immobilized lipid chromatography (ILC),18 second harmonic generation (SHG), ¹¹ Fourier transform infrared spectroscopy (FTIR), ¹⁹ NMR, ²⁰ fluorescence emission, ^{21,22} and differential scanning calorimetry (DSC). 23 Partitioning of 12 anthracyclines, anticancer drugs, was studied through relating general fluorescence intensity to partitioning depth in the membrane. This study showed that the partition coefficient of anthracyclines in large unilamellar vesicles (LUVs) was generally related to the drug's hydrophobicity.²⁴ Nguyen and Conboy measured the binding affinity of tetracaine as a function of lipid physical state using SHG. The binding affinity of tetracaine to liquid crystalline state DMPC and DPPC (46 °C) was 5,500 M⁻¹ and 2,400 M⁻¹, respectively. Binding of tetracaine to gel state DMPC and DPPC bilayers could not be quantitatively assessed, however, as signal levels were below detection limits. 11 Liu and co-workers used ILC to determine temperature effects on solute-membrane partitioning. Of 15 drugs studied, membrane partitioning coefficients increased over a broad temperature range, while the partitioning coefficients of four drugs (including three beta blockers) decreased. 18

While these techniques all provide a general framework for describing solute—membrane interactions, time resolved fluorescence measurements used in the experiments described below have distinct advantages. Specifically, time resolved fluorescence enables determination of the precise location of solutes within a lipid membrane. The time-resolved measurements described below also allow for the quantification of solute partitioning and how partitioning changes as the physical state of the membrane is altered. Moreover, quantitative fluorescence measurements allow for a thermodynamic analysis of solute partitioning in DPPC membranes, providing both enthalpic and entropic data that imply changes in partitioning mechanism(s) as the phase of the lipid bilayer changes.

In experiments described below, we investigate the partitioning of C152 and C461 in DPPC membranes. Both coumarins used in this work are N_1N -dimethyl-substituted tertiary amines. Coumarin 152 (C152) has an electron withdrawing -CF3 group in the 4-position, while coumarin 461 (C461) has a weak electron donating -CH3 group in the 4-position (Chart 1). Both molecules are hydrophobic, with C152 having slightly more hydrophobic character (log P = 2.72) than C461 (log P = 2.29) due to the trifluoromethyl group. (log P values were calculated using ChemDrawPrime 16.0.) The ground state dipole moments of C152 and C461 are identical

Chart 1. Molecular structures of (top) coumarin 152 (C152) and (bottom) coumarin 461 (C461)

(6.3 D), while the excited state dipole moment of C152 (12.8 D) is slightly higher than that of C461 (10.0 D). 25 Partitioning of C152 and C461 in DPPC membranes is quantified as a function of bulk C152 concentration as well as the ratio of concentration to DPPC vesicles in solution. Time-correlated single photon counting (TCSPC) fluorescence spectroscopy is used to determine the relative percent of solutes present in distinct lipid vesicle microenvironments. Fluorescence traces are fit to a multiexponential model, with three distinct lifetimes representing the solute in bulk buffer, near the polar lipid headgroups, and in the nonpolar lipid bilayer core. Additional details of this analysis can be found in previous reports and in the Supporting Information. 22,26

Results presented below quantitatively measure C152 and C461 partitioning into phosphocholine membranes above and below each membrane's gel-liquid crystalline transition temperature. Furthermore, characteristic photophysical behaviors are used to clarify where solutes partition within a model membrane at different temperatures. Data show that the absolute number of C152 solutes associated with DPPC membranes is approximately an order of magnitude higher than the number of C461 solutes associated with DPPC membranes. Results presented here expand and quantify findings from previous studies investigating C152 partitioning in phosphocholine membranes.²¹ Furthermore, the approach to characterizing and quantifying solute partitioning into membranes is sufficiently general so that it can be applied to a wide range of naturally fluorescent molecules used in biomedical and environmental applications.²⁷

EXPERIMENTAL METHODS

Materials. 1,2-Dipalmitoyl-sn-glycero-3-phosphocholine (16:0 DPPC) was purchased in powder form from Avanti Polar Lipids (Alabaster, AL, USA). Laser grade coumarin 152 and coumarin 461 were purchased from Exciton (Dayton, OH, USA). Millipore water (18.2 M Ω) was used to make phosphate-buffered saline. Solvents were purchased from Sigma-Aldrich. All materials were used as received.

Large Unilamellar Vesicle Preparation. Large unilamellar vesicles (LUVs) were prepared according to the procedure described previously.³¹ Briefly, DPPC was dissolved in chloroform and subsequently removed via rotary evaporation, creating a thin lipid film. The film was rehydrated using 10 mM phosphate-buffered saline (PBS, pH = 7) to form a 1.5 mM lipid vesicle suspension. The suspension was sonicated for 30 min at ~50 °C. The solution was then passed through a PTFE

syringe filter (450 nm) to remove the giant unilamellar vesicles, subsequently heated (~50 °C), and passed through an Avanti Mini Extruder (membrane pore size of 200 nm) 10 times. This procedure resulted in a distribution of vesicles having diameters measuring approximately 210 nm in diameter with a small population having markedly smaller diameters (60 nm).

Time-Correlated Single Photon Counting. Time-resolved fluorescence emission data were collected using Picoquant PicoHarp 300 and FluoTime 200 software. An APE Autotracker containing a SHG crystal situated after a Chameleon laser (Coherent, 80 MHz, 680–1080 nm) produced excitation pulses (85 fs pulse width) at a wavelength of 400 nm. A Conoptics Model 350-105 modulator maintained a 4 MHz pulse repetition rate. Sample temperatures were maintained by a Quantum Northwest TC152 temperature control. A long-pass filter (80% transmission >455 nm) was placed after the sample to reduce scattering from vesicles in solution. Photon emission was collected at 500 nm. Additional details about this assembly can be found in previous reports. ^{21,26,32}

In a given TCSPC experiment, signal was collected until the maximum intensity at early times reached a threshold of 8000 counts. Depending on the local solvation environment of the solute (and thus radiative rate and fluorescence quantum yield), the time required for each experiment varied with temperature. The instrument response function was accounted for by reconvolution of each experiment's raw data, and fluorescence decays were fit to a sum of decaying exponentials terms corresponding to independent radiative lifetimes:

$$I(t) = \int_{-\infty}^{t} IRF(t') \sum_{i=1}^{n} A_{i} e^{-(t-t')/\tau_{i}} dt'$$
(1)

In eq 1, A_i is the amplitude of component i and τ_i is the lifetime of component i. Each trace was fit independently without any constraints on lifetimes or amplitudes. Typical χ^2 values ranged from 0.90 to 1.10. The corrected Akaike information criterion (AIC), described elsewhere, ³³ was used to determine the ideal number of fluorescence lifetimes in each data set. For C152 in DPPC vesicle solutions, this model consistently recommended three fluorescence lifetimes, while two fluorescence lifetimes were recommended for C461 in DPPC vesicle solutions. Additional information about this data analysis can be found in the Supporting Information.

The local environments sampled by C152 and C461 in vesicle containing solutions are identified from each fluorescence lifetime and correlated with an equivalent bulk solvent having a quantitatively similar lifetime. The amplitudes associated with individual lifetimes are then corrected for the radiative rate of C152 or C461 in each assigned environment. The resulting amplitudes are normalized, producing the fractional lifetime contribution.

DPPC Titrations. To further quantify the partitioning behavior of C152 and C461 in DPPC vesicles, DPPC vesicles were slowly titrated into a coumarin/buffer solution. The fluorescence emission of the coumarin/buffer solutions were recorded from 10 to 70 °C. A DPPC vesicle solution (1.5 mM) was titrated stepwise into the bulk C152 or C461 solutions. With each step of the titration, fluorescence emission of the solution was recorded from 10 to 70 °C.

RESULTS AND DISCUSSION

Fluorescence absorbance and emission of C152 and C461 in bulk solvents are shown in Tables 1 and 2. Four solvents were

Table 1. Photophysical Properties of C152 in Selected Solvents at 10 $^{\circ}$ C

solvent	$(nm)^a$	$(nm)^a$	$k_{\rm f} (10^7 { m s}^{-1})$	$arphi_{ m f}$	$\tau_{\rm f}~({\rm ns})^b$
cyclohexane	372	426	25.1	0.97 ^c	3.86
acetonitrile	396	502	9.8	0.23^{d}	2.34
methanol	397	515	9.0	0.09 ^c	1.09
0.01 M PBS buffer	404	527	8.1	0.05 ^d	0.62 (0.83), 3.75 (0.17)

^aMeasured at room temperature. ^bUncertainties in reported lifetimes are ± 0.10 ns. Uncertainties in reported amplitudes (for the PBS buffer solution) are ± 0.05 . ^cQuantum yields as reported by Pal et al. ³⁴. ^dQuantum yields measured in this work. Experiments were conducted at room temperature and remain virtually unchanged from 10 to 70 °C.

Table 2. Photophysical Properties of C461 in Selected Solvents at 10 $^{\circ}\text{C}$

solvent	$\frac{\lambda_{\rm exc}}{({\rm nm})^a}$	$\frac{\lambda_{\rm em}}{({\rm nm})^a}$	$k_{\rm f} (10^7 { m s}^{-1})$	$arphi_{ m f}^{m b}$	$\tau_{\rm f}~({\rm ns})^c$
cyclohexane	349	390	31.9	0.82	2.57
acetonitrile	363	431	14.7	0.55	3.73
methanol	368	451	13.6	0.46	3.38
0.01 M PBS buffer	372	473	5.4	0.08	1.48 (0.92), 5.13 (0.08)

"Measured at room temperature. b Quantum yields measured in this work. Experiments were conducted at room temperature and remain virtually unchanged from 10 to 70 °C. CUncertainties in reported lifetimes are ± 0.10 ns. Uncertainties in reported amplitudes (for the PBS buffer solution) are ± 0.05 .

chosen to represent the different fluorescence environments C152 and C461 may encounter in a lipid vesicle solution: cyclohexane (hydrophobic membrane interior), acetonitrile and methanol (polar regions near the lipid headgroups), and buffer (unassociated with the vesicle or fully solvated within the water pool inside the vesicle).

Fluorescence emission decay traces of C152 and C461 in bulk solvents are shown in Figure 1. Fluorescence lifetimes of C152 vary systematically with solvent polarity. C152 in buffer is fit to two exponential decays, with a large contribution due to a fast (\sim 0.5 ns) decay. In polar solvents such as methanol and acetonitrile, the fluorescence lifetime is longer (\sim 1–2 ns), while, in nonpolar solvents, fluorescence decay is significantly longer (\sim 4 ns). A correlation between fluorescence lifetime and solvent polarity is not observed for C461 although C461 lifetimes in different solutes remain distinguishable from each other.

The slight difference in molecular structure of C461 and C152 creates distinctly different fluorescence behaviors depending on local solvation environments. In nonpolar solvents, both C152 and C461 have a nonpolar structure. Excitation of C152 and C461 in these solvents produces no charge separation, resulting in long fluorescence lifetimes (~4 ns and ~2.5 ns, respectively). Upon excitation in polar solvents, C152 accesses a twisted intramolecular charge transfer state (TICT). The presence of this state is evidenced by a small quantum yield (and a large nonradiative rate). In the same

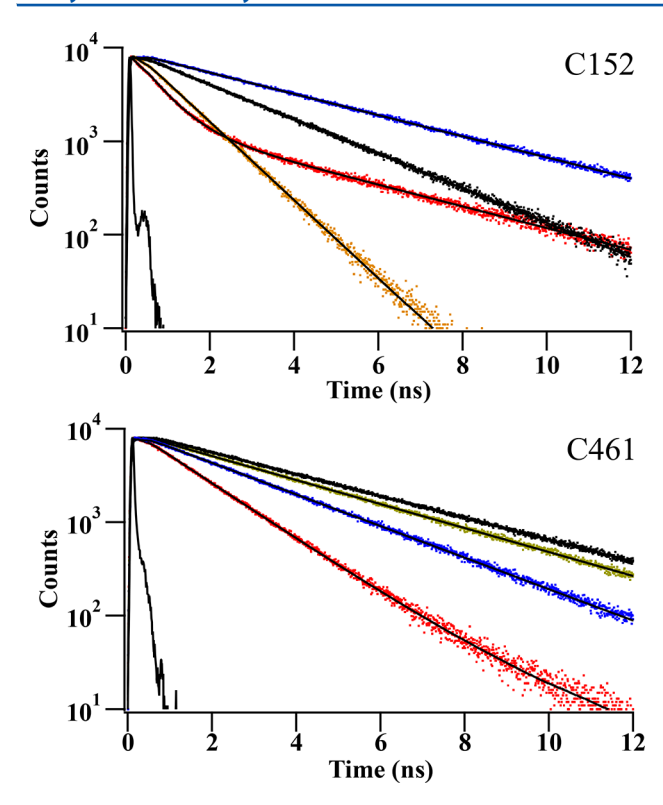


Figure 1. Fluorescence traces of C152 and C461 in buffer (red), acetonitrile (black), methanol (orange), and cyclohexane (blue). All fluorescence traces were recorded at 10 °C.

polar solvents, C461 is *not* able to access this TICT state, due to the lack of the electron withdrawing -CF₃ group.

When C152 and C461 are added individually to DPPC vesicle solutions, fluorescence lifetime behaviors change dramatically (Figure 2), indicating that vesicles are providing

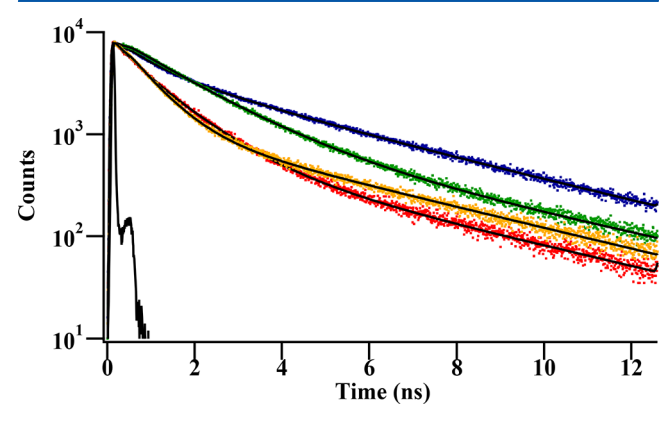


Figure 2. Fluorescence traces of C152 in DPPC solutions at 10 °C (dark blue, top) and 70 °C (red, bottom), and C461 in DPPC vesicles solutions at 10 °C (green, second from top) and 70 °C (orange, second from bottom).

solutes with heterogeneous solvation environments. The fluorescence decay of C152 in DPPC solution is best fit to three lifetimes, while emission decay of C461 in DPPC vesicles is best fit to two lifetimes.

As the temperature is raised from 10 to 70 °C, fluorescence decays of C152 in DPPC vesicle solutions are fit to a short lifetime (τ_1 = ~0.5 ns), an intermediate lifetime (τ_2 = ~1.5 ns), and a long lifetime (τ_3 = 4 ns) (Figure 3). Due to their

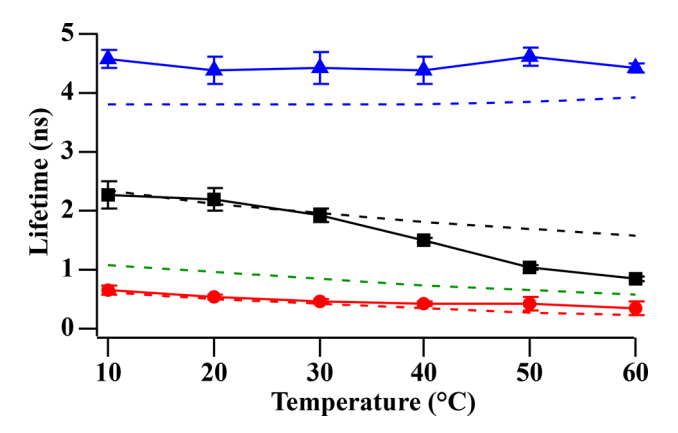


Figure 3. Fluorescence lifetimes of C152 in bulk solvents represented by dashed lines: cyclohexane (blue), acetonitrile (black), methanol (green), and buffer (red). The long (minor) lifetime of C152 in buffer is omitted. The three lifetimes of C152 in DPPC vesicles are represented by blue triangles (τ_3 , nonpolar), black squares (τ_2 , polar), and red circles (τ_1 , buffer).

similarities with lifetimes measured in bulk solvents over the range of temperatures sampled, τ_1 and τ_3 are assigned to C152 solvated in bulk aqueous solution and in the nonpolar, hydrophobic bilayer interior, respectively. Only the intermediate lifetime, τ_2 , changes significantly with temperature, shortening from 2.15 ns at 10 °C to 1.03 ns at 70 °C. The C152 population with this lifetime is assigned to solutes in the solvation environment created by the DPPC glycero backbone region of the DPPC vesicles. As the lipid bilayer becomes more fluid and permeable to water, τ_2 moves from a value consistent with solvation in a polar aprotic environment to the polar protic limit. This change is believed to reflect increased hydrogen bonding within the bilayer interior as water begins to permeate the headgroup region. ³⁵

Fluorescence decay traces of C461 in DPPC vesicle solutions were fit to a short ($\tau_1 = \sim 1$ ns) and a long ($\tau_2 = \sim 4.8$ ns) lifetime. As shown in Figure 4, τ_1 of C461 in DPPC vesicle

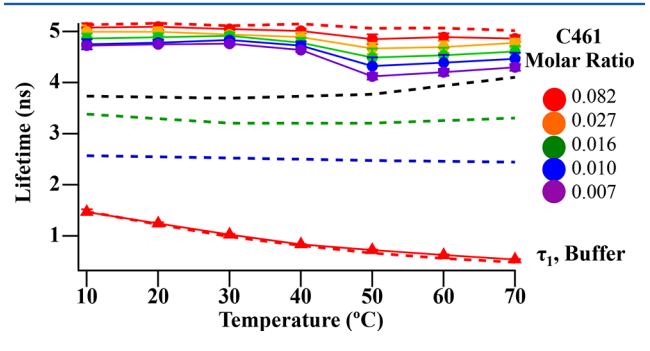


Figure 4. Fluorescence lifetimes of C461 in bulk solvents represented by dashed lines: cyclohexane (blue), acetonitrile (black), methanol (green), and buffer (red). The short lifetime (τ_1) of C461 in DPPC solutions is shown with solid red triangles. The longer lifetime of C461 in DPPC solutions is shown with circles from 4–5 ns.

solutions tracks the dominant short lifetime of C461 in buffer. τ_2 of C461 in the DPPC vesicle solutions is most similar to the long (minor amplitude contribution) lifetime of C461 in buffer solution. However, τ_2 of C461 associated with DPPC vesicles decreases noticeably between 40 and 50 °C. Since the melting temperature of DPPC vesicles is in this temperature range, we have assigned this C461 lifetime to solutes associated with the

vesicle. This hypothesis is further confirmed by the trend in fluorescence traces of C461 occurring at lower molar ratios: as the amount of DPPC vesicles present in solution increases, we see τ_2 's amplitude decrease even more significantly in the vicinity of the lipid bilayer transition temperature.

Molecular dynamics simulations of fully hydrated DPPC bilayers in their liquid crystalline state have provided some insight into the electrostatic interactions occurring in the headgroups of the lipids. When fully hydrated, the charge densities of the choline and phosphate groups are completely compensated for by the charge density of the dipoles of the surrounding waters (11–16 water molecules).³⁶

To quantify partitioning of C152 and C461 in DPPC vesicles, DPPC vesicles were slowly titrated into a coumarin/buffer solution. The fluorescence emission of 2.5 mL of C152 (3.73 μ M) was recorded from 10 to 70 °C. A DPPC vesicle solution (1.5 mM) was titrated stepwise into the bulk C152. With each step of the titration, fluorescence emission of the solution was recorded from 10 to 70 °C. A DPPC vesicle solution was added in five steps, corresponding to C152:DPPC lipid ratios of 0.0009, 0.001, 0.002, 0.005, 0.008, 0.012, 0.021, and 0.062. The corresponding C152 concentrations in these solutions were 1.07, 1.24, 1.74, 2.52, 2.83, 3.11, 3.33, and 3.59 μ M. However, in related partitioning studies, 37,38 concentrations are reported as solute:lipid ratios, and that convention is adopted in the discussion below.

To observe the change in C152 partitioning with temperature, the fluorescence decay data were fit to three lifetimes and associated amplitudes using eq 1. The raw amplitudes of the fluorescence decays were corrected by the radiative rates of C152 in buffer (τ_1) , methanol/acetonitrile (τ_2) , and cyclohexane (τ_3) . The resulting radiative rate corrected amplitudes were then normalized, resulting in the percent of C152 molecules in each environment. A more detailed description of this analysis is included in Supporting Information.

Figure 5 shows partitioning of C152 into DPPC vesicles as a function of both C152:DPPC vesicle mole ratio and temper-

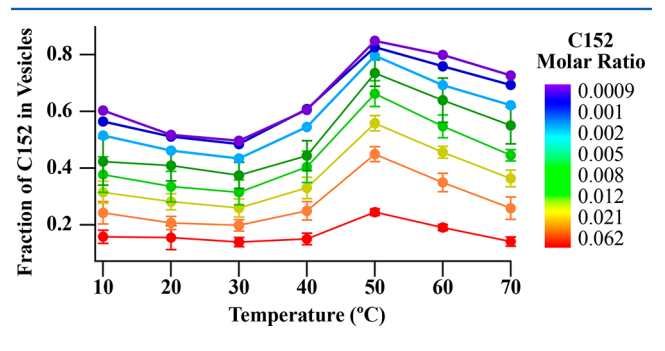


Figure 5. Membrane partitioning of C152 in DPPC vesicles as a function of solution temperature and C152:DPPC molar ratio. C152 molar concentration decreases from red to purple.

ature. The fraction of C152 in vesicles comprises the sum of the amplitudes associated with the intermediate (τ_2 , polar environment) and long lifetimes (τ_3 , nonpolar environment). At all temperatures, the fraction of C152 in the vesicle depends on the amount of C152 in the solution. As more DPPC is titrated into the solution, we observe an increase in C152 partitioning into the vesicles. We also observe an increase in partitioning near the melting temperature (42 °C). The percent of C152 in the vesicle reaches a maximum near 50 °C, and C152

exsolvation from the membrane is observed as the temperature increases to 70 $^{\circ}\text{C}.$

C461 (4.11 μ M):DPPC (1.5 mM) vesicle titrations were conducted in a manner similar to the C152:DPPC titrations described above. The C461:DPPC lipid ratios were 0.007, 0.010, 0.016, 0.027, and 0.082. These ratios correspond to bulk C461 concentrations of 2.94, 3.24, 3.52, 3.74, and 3.98 μ M. C461/DPPC fluorescence traces were fit to two lifetimes. The short lifetime, τ_1 , remains identical (within error) to the short lifetime of C461 in a pure buffer solution (Figure 4), and therefore C461 with this fluorescence decay is assumed to remain unassociated with the DPPC membrane. The long lifetime of C461 in the DPPC membrane (τ_2) was attributed to C461 associated with the vesicle membrane. The amplitudes associated with τ_1 and τ_2 were corrected for the radiative rates of C461 in buffer and acetonitrile, respectively, to determine partitioning ratios.

The percent of membrane-associated C461 was plotted as a function of molar ratio and temperature (Figure 6). Below the

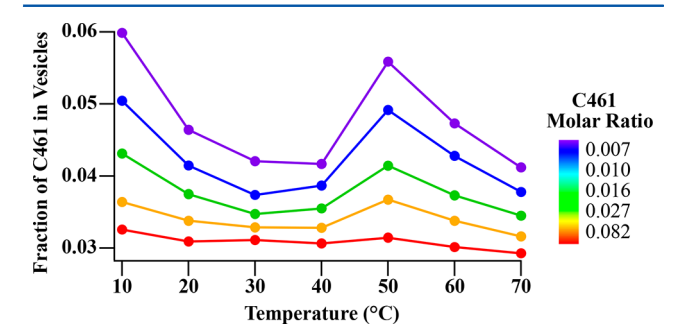


Figure 6. Membrane partitioning of C461 in DPPC vesicles as a function of solution temperature and C461:DPPC molar ratio.

melting temperature of DPPC, the trend in partitioning differs from that of C152 in the same temperature range. At the lowest temperature (10 °C), C461 association with the membrane is relatively large at the lowest molar ratios (relative to the other temperatures investigated), although still much less than C152 partitioning at any temperature. As the temperature increases toward the melting temperature, C461 dissociates from the membrane into solution, suggesting that C461's interactions with the lipid bilayer do not involve solvation within the polar headgroup region and instead result from a nonspecific, surface adsorption. This trend is most pronounced at low C461:DPPC mole ratios. Similar to the behavior of C152 in DPPC vesicles, an increase in association is observed at DPPC's melting temperature. Above 50 °C, we once again observe C461 exsolvation from the membrane.

The most striking result of these coumarin/DPPC titration experiments is the difference in magnitude of membrane association. At all temperatures investigated, the average absolute number of C152 molecules associated with vesicles is an order of magnitude larger than the average number of C461 molecules associated with each vesicle. To visualize this comparative partitioning, data presented in Figures 5 and 6 can be used to determine the number of coumarins partitioning into vesicle membranes (as a function of temperature and mole concentration). Using several coarse approximations, the number of vesicles in solution was determined using the DPPC monomer concentration. Assuming a spherical vesicle with an average 200 nm diameter, an average bilayer thickness of 4 nm, ³⁹ and an average DPPC molecular area of 57 Å², ⁴⁰

each DPPC vesicle is calculated to contain ~400,000 DPPC molecules. With these assumptions and following the concentrations of coumarins and DPPC solutions for each titration, we calculated the average number of coumarins per vesicle at different coumarin molar concentrations (Figure 7).

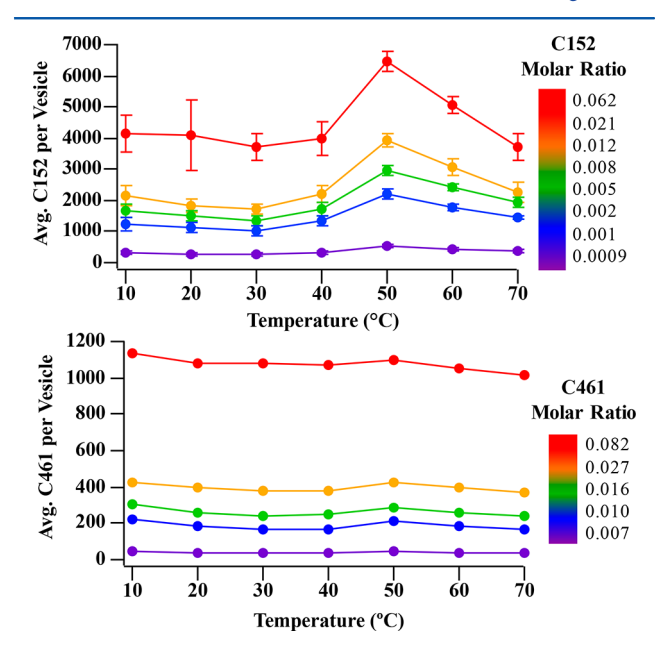


Figure 7. Average number of C152 (top) and C461 (bottom) molecules per vesicle as a function of temperature. Colored traces indicate the molar ratio of coumarins to DPPC lipids.

At first, Figures 5 and 6 appear to contradict Figure 7. Figures 5 and 6 show that at higher mole ratio of coumarins to DPPC lipids, a smaller percent of coumarin solutes associate with vesicles. Figure 7 and Table 3 clarify this apparent

Table 3. Average Number of C152 and Percent of C152 per Vesicle in Select Steps of the C152:DPPC Titration^a

mole ratio	$[C152]_{ ext{bulk}} \ (\mu ext{M})$		10 °C	30 °C	50 °C	70 °C
0.062	3.59	av no. C152	4200	3700	6500	3700
		% C152	16	14	25	14
0.008	2.83	av no. C152	1200	1000	2200	1500
		% C152	38	32	66	45
0.002	1.74	av no. C152	500	400	700	600
		% C152	52	43	80	62
0.0009	1.07	av no. C152	300	200	400	300
		% C152	60	50	85	73

"Error in the percent of C152 in vesicles is typically <3%, and error in the average number of C152 per vesicle is typically <10%. A full analysis including individual errors is provided in the Supporting Information.

contradiction by showing that as the number of DPPC vesicles in solution increases, the number of coumarins associated with each vesicle also increases. A similar table for the C461 titration appears in the Supporting Information.

At all C152 molar concentrations investigated, the percent of C152 that partitions into the vesicle is strongly temperature-dependent (+30% increase in partitioning from gel to liquid crystalline). (Data for additional molar ratios are shown in the Supporting Information.) Figure 8 also shows that, at a given

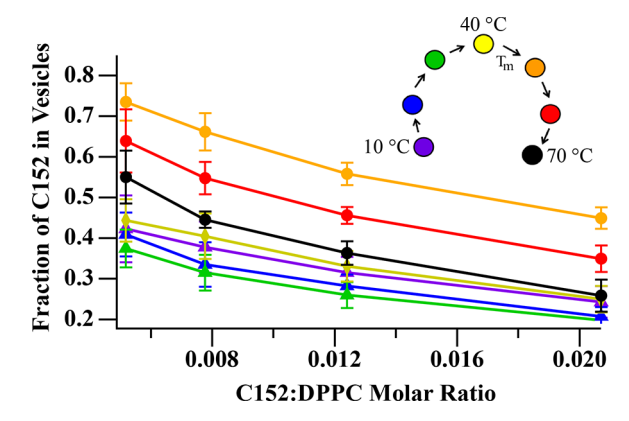


Figure 8. Percent of C152 population solvated in the DPPC bilayer plotted as a function of C152:DPPC molar ratio. Colored traces indicate solvation at 10 °C (purple), 20 °C (blue), 30 °C (green), 40 °C (yellow), 50 °C (orange), 60 °C (red), and 70 °C (black).

mole fraction, C152 partitioning remains similar at all temperatures below the melting temperature. Based on the similarity between the traces at 30 and 40 $^{\circ}$ C, no evidence of any change in partitioning accompanies the DPPC structural change at the pretransition temperature (35 $^{\circ}$ C). This result implies that changes in bilayer structure and fluidity accompanying the pretransition are not significant enough to induce any changes in partitioning behavior.

C152 partitioning into DPPC vesicles can also be visualized as a partitioning constant (K_{part}) of C152 in the aqueous phase and the lipid phase as a function of the C152 mol ratio (Figure 9).

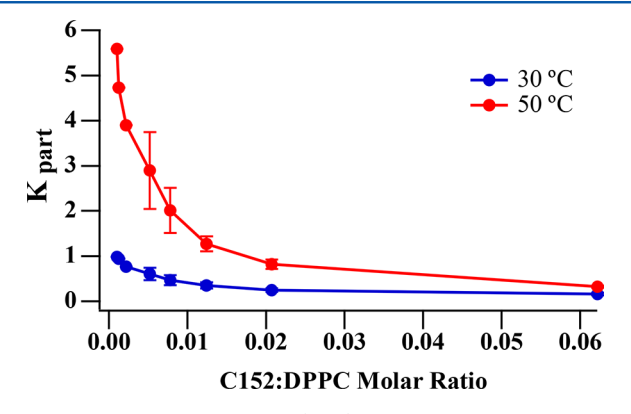


Figure 9. Partitioning coefficient ($K_{\rm part}$) of C152 in DPPC vesicles as a function of C152:DPPC molar ratio. Red traces indicate partitioning coefficients of C152 into liquid crystalline phase membranes (50 °C), and blue traces indicate partitioning coefficients of C152 into gel phase membranes (30 °C).

Regardless of the mole ratio of C152:DPPC in Figure 9, $K_{\rm part}$ of the solution at 50 °C remains larger than $K_{\rm part}$ of the solution at 30 °C. Furthermore, data recorded below the melting temperature of the vesicles (42 °C) show little dependence on the mole ratio of C152:DPPC. These results demonstrate clearly that when DPPC is in its gel phase, the ratio of C152 in the lipid bilayer to aqueous buffer remains constant, regardless of temperature. Most interesting is the drastic change in the partition coefficient of C152 in DPPC vesicles as a function of C152:DPPC molar ratio. At high molar ratios, the partitioning coefficient in both the gel and the liquid crystalline phases decreases toward zero as one would expect in the limit of excess

C152 bulk solution concentrations. As the C152:DPPC molar ratio decreases, we see an exponential increase in the partition coefficient, indicating that the solution is starting to approach the dilute solute limit. At infinitely dilute C152 mole ratios, we expect $K_{\rm part}$ to be on the order of ~500 (as predicted by the log P of C152).

Thermodynamic Analysis. A van't Hoff analysis (Figure 10) was used to calculate the enthalpic and entropic

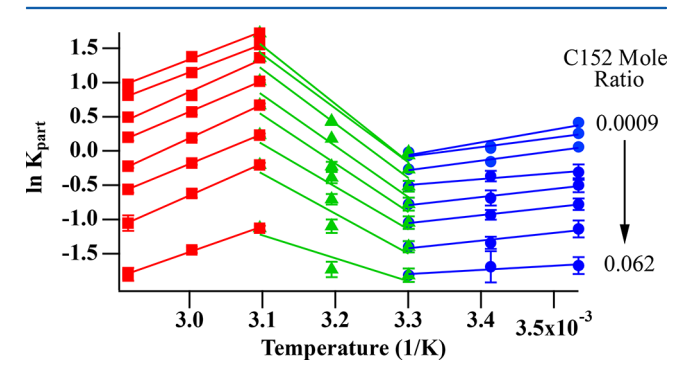


Figure 10. van't Hoff analysis of C152 partitioning into DPPC vesicles as a function of temperature. The colors indicate the temperature range (blue circles) below DPPC melting temperature, (green triangles) near the transition temperature of DPPC, and (red squares) above the melting temperature. C152:DPPC mole ratios decrease with increasing partition coefficients.

contributions to the thermodynamics of C152 membrane permeation. Partitioning is analyzed as a function of the amount of C152 in the lipid membrane relative to the amount C152 in the aqueous phase (K_{part}) .

The partitioning is further analyzed in terms of the enthalpic and entropic contributions to the overall C152 partitioning thermodynamics (Figure 11 and Table 4). (A similar analysis for C461 appears in the Supporting Information.)

Entropic and enthalpic contributions to membrane partitioning vary significantly with the physical phase of the membrane. Below the melting temperature of DPPC, C152 partitioning is slightly exothermic and entropically favored. Small enthalpic contributions to partitioning in gel phase membranes have similarly been reported throughout literature. Kwon et al. investigated the partitioning of 16 endocrine disrupters in gel phase DPPC membranes. Fourteen of the selected solutes showed entropic driven partitioning (~5–55 J/(mol·K)) with a small endothermic contribution (2–30 kJ/mol). Rogers and Davis found the partitioning of four *p*-alkylphenols in gel phase DMPC membranes to be endothermic (~1–9 kJ/mol) and slightly entropically favorable (65–75 J/(mol·K)).

Near DPPC's melting temperature we observe a large entropically driven increase in partitioning, with a large endothermic contribution. In this temperature range, small changes in temperature create large structural changes within the bilayer, including an increase in volume (~4%), area (15–25%), ⁴³ and enthalpy (20–40 kJ/mol). ⁴⁴ The structural changes in the membrane coincide with large lateral lipid density fluctuations. We attribute the increase in membrane partitioning in this narrow temperature region to result from these enhanced fluctuations.

Above the melting temperature, we observe C152 exsolvation from the membrane back into buffer driven by a relatively large exothermic ΔH_{part} , a result similar to findings in numerous other studies, van Wezel et al. investigated partitioning of a

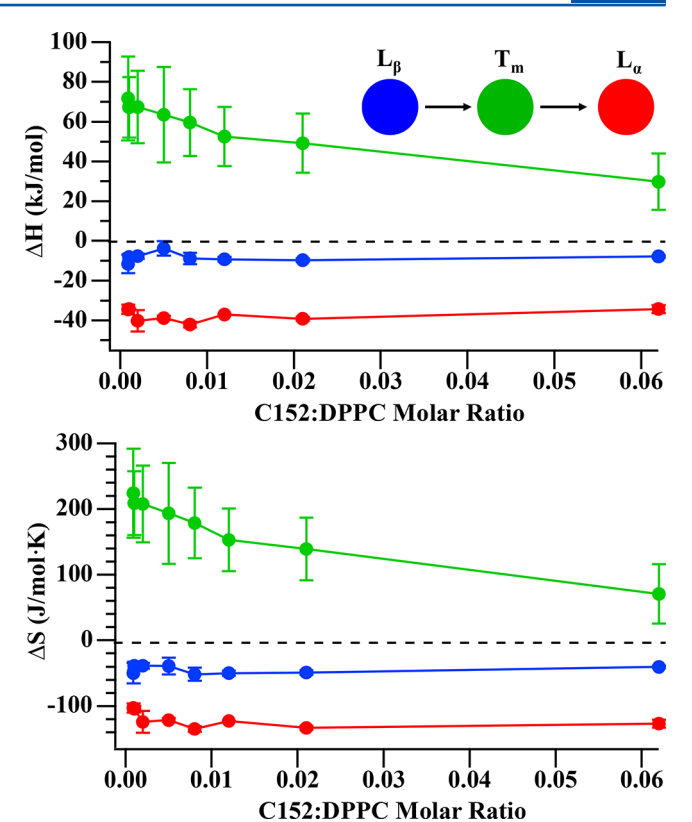


Figure 11. Enthalpy (top) and entropy (bottom) of C152 partitioning into DPPC vesicles as a function of C152:DPPC molar ratio. The three lines in each figure indicate the temperature range (blue) below DPPC's melting temperature, (green) near the transition temperature of DPPC, and (red) well above the melting temperature.

series of chlorobenzenes partitioning into DPPC vesicles in the liquid crystalline phase. For all seven analogues studied, partitioning was exothermic (~-10 to -30 kJ/mol) and slightly entropically favored (20–60 J/(mol·K)). 45 Partitioning of paclitaxel, an anticancer drug, into liquid crystalline POPC vesicles was found to be exothermically driven (-105 kJ/ mol).46 Partitioning of three indole derivatives into liquid crystalline POPC membranes was similarly found to be exothermic (-21 to -30 kJ/mol) and slightly entropically favorable $(10-40 \text{ J/(mol \cdot K)})$. Given the complexity of these systems, assigning physical mechanisms to these thermodynamic quantities is a speculative exercise at best, so we are reluctant to overinterpret the specific magnitudes and signs of partitioning enthalpy and entropy in these different membrane regimes. In this context, molecular dynamic simulations that separate different thermodynamic contributions to the system's overall free energy would be advantageous in both testing the results presented in this work and identifying the most important processes that control solute partitioning into lipid membranes.

CONCLUSIONS

Data presented in this work have shown the similarities and differences in temperature-dependent partitioning of coumarin 152 and coumarin 461 in DPPC lipid vesicles. Results indicate that C152 has a \sim 10-fold greater affinity than C461 for lipid bilayers, despite both solutes having similar hydrophobicities as calculated from their log P values. The increase in membrane affinity is attributed to the presence of a -CF₃ group present in

Table 4. Temperature-Dependent Enthalpy and Entropy Contributions to C152 Partitioning in DPPC Membranes

		$T < T_{\rm m}$		$T \sim T_{\rm m}$		$T > T_{\rm m}$	
bulk C152 concn (µM)	molar ratio (C152:DPPC)	ΔH (kJ/mol)	ΔS (J/mol K)	ΔH (kJ/mol)	ΔS (J/mol K)	ΔH (kJ/mol)	ΔS (J/mol K)
3.59	0.062	-5 ± 2	-32 ± 8	19 ± 13	76 ± 41	-31 ± 2	-105 ± 5
3.33	0.021	-9 ± 3	-43 ± 10	48 ± 15	147 ± 48	-39 ± 1	-123 ± 3
3.11	0.012	-10 ± 1	-41 ± 2	52 ± 15	161 ± 48	-37 ± 1	-111 ± 1
2.83	0.008	-10 ± 2	-39 ± 6	59 ± 17	186 ± 54	-41 ± 1	-122 ± 4
2.52	0.005	-7 ± 2	-28 ± 7	62 ± 24	199 ± 76	-38 ± 1	-108 ± 4
1.74	0.002	-12 ± 2	-40 ± 6	66 ± 19	214 ± 60	-40 ± 5	-113 ± 16
1.24	0.001	-11 ± 2	-38 ± 7	65 ± 16	215 ± 50	-34 ± 1	-93 ± 4
1.07	0.0009	-15 ± 5	-52 ± 17	70 ± 21	231 ± 68	-34 ± 2	-92 ± 7

the 4-position of C152. Results presented here support several other empirical studies that link drug halogenation to increased membrane affinity. An important contribution from work described here is the quantitation of dissolved solute accommodated by vesicles as a function of solution temperature and solute concentration. We expect that similar information can come from related systems provided that the solute of interest has well-defined properties that are distinctly sensitive to heterogeneous solvation environments.

Temperature-dependent partitioning data were also used to calculate enthalpies and entropies of C152 partitioning as a function of concentration. These values were used to extrapolate these quantities in the infinitely dilute limit. Above and below the lipid gel–liquid crystalline temperature, partitioning is exothermic with negative changes in entropy. In the vicinity of the transition temperature, these quantities change sign with $\Delta H_{\rm part}$ becoming endothermic (+40–70 kJ/mol) and $\Delta S_{\rm part} = +100-200$ J/(mol·K). Enthalpic and entropic contributions represent a sensitive balance between solute solvation in the lipid membrane or bulk aqueous buffer. Also contributing to these thermodynamics are the energetic costs (or gains) due to membrane disruption (solute insertion) or reordering (solute exsolvation).

ASSOCIATED CONTENT

Supporting Information

The Supporting Information is available free of charge on the ACS Publications website at DOI: 10.1021/acs.analchem.7b03964.

Data analysis methods; complete analysis of solute:vesicle and percent of membrane-associated solute in vesicle solutions; thermodynamic analysis for C461 in DPPC vesicle solutions (PDF)

AUTHOR INFORMATION

Corresponding Author

*E-mail: rawalker@montana.edu. Fax: +1 406-994-5401.

ORCID ®

Robert A. Walker: 0000-0002-0754-6298

Notes

The authors declare no competing financial interest.

ACKNOWLEDGMENTS

This work was supported originally, in part, by the National Science Foundation (Grants CHE-1040294 (MRI) and CHE-1710695) and by the Montana Research and Economic Development Initiative.

REFERENCES

- (1) van Wezel, A. P.; Opperhuizen, A. Crit. Rev. Toxicol. 1995, 25, 255-279.
- (2) Geyer, H. J.; Rimkus, G. G.; Scheunert, I.; Kaune, A.; Schramm, K.-W.; Kettrup, A.; Zeeman, M.; Muir, D. C.; Hansen, L. G.; Mackay, D. In *Bioaccumulation—New Aspects and Developments*; Beek, B., Ed.; The Handbook of Environmental Chemistry, Vol. 2, Part J; Springer: Berlin, 2000; p 1–166.
- (3) Jørgensen, K.; Ipsen, J. H.; Mouritsen, O. G.; Zuckermann, M. J. Chem. Phys. Lipids 1993, 65, 205–216.
- (4) DiMagno, S. G.; Sun, H. Curr. Top. Med. Chem. 2006, 6, 1473-1482.
- (5) Gerebtzoff, G.; Li-Blatter, X.; Fischer, H.; Frentzel, A.; Seelig, A. ChemBioChem 2004, 5, 676–684.
- (6) Wang, J.; Sánchez-Roselló, M.; Aceña, J. L.; del Pozo, C.; Sorochinsky, A. E.; Fustero, S.; Soloshonok, V. A.; Liu, H. *Chem. Rev.* **2014**, *114*, 2432–2506.
- (7) Müller, K.; Faeh, C.; Diederich, F. Science 2007, 317, 1881-1886.
- (8) Hernandes, M. Z.; Cavalcanti, S. M. T.; Moreira, D. R. M.; de Azevedo Junior, W. F.; Leite, A. C. L. Curr. Drug Targets 2010, 11, 303-314
- (9) Blicher, A.; Wodzinska, K.; Fidorra, M.; Winterhalter, M.; Heimburg, T. *Biophys. J.* **2009**, *96*, 4581–4591.
- (10) Nagle, J.; Scott, H. Biochim. Biophys. Acta, Biomembr. **1978**, 513, 236–243.
- (11) Nguyen, T. T.; Conboy, J. C. Anal. Chem. 2011, 83, 5979-5988.
- (12) Wright, S. E.; White, J. C.; Huang, L. Biochim. Biophys. Acta, Biomembr. 1990, 1021, 105–113.
- (13) Bemporad, D.; Luttmann, C.; Essex, J. Biochim. Biophys. Acta, Biomembr. 2005, 1718, 1–21.
- (14) Bemporad, D.; Luttmann, C.; Essex, J. *Biophys. J.* **2004**, 87, 1–13.
- (15) Lipinski, C. A.; Lombardo, F.; Dominy, B. W.; Feeney, P. J. Adv. Drug Delivery Rev. 1997, 23, 3–25.
- (16) Lipinski, C. A. J. Pharmacol. Toxicol. Methods 2000, 44, 235–249.
- (17) Seelig, A.; Gatlik-Landwojtowicz, E. Mini-Rev. Med. Chem. 2005, 5, 135–151.
- (18) Liu, X.-Y.; Yang, Q.; Kamo, N.; Miyake, J. J. Chromatogr. 2001, 913, 123-131.
- (19) Chen, C.; Tripp, C. P. Biochim. Biophys. Acta, Biomembr. 2008, 1778, 2266–2272.
- (20) Gao, P.; Fagerness, P. E. Pharm. Res. 1995, 12, 955-964.
- (21) Gobrogge, C. A.; Kong, V. A.; Walker, R. A. J. Phys. Chem. B **2016**, 120, 1805–1812.
- (22) Gobrogge, C. A.; Kong, V. A.; Walker, R. A. J. Phys. Chem. B **2017**, 121, 7889–7898.
- (23) Zhang, F.; Rowe, E. S. Biochemistry 1992, 31, 2005-2011.
- (24) Gallois, L.; Fiallo, M.; Laigle, A.; Priebe, W.; Garnier-Suillerot, A. Eur. J. Biochem. **1996**, 241, 879–887.
- (25) Rechthaler, K.; Köhler, G. Chem. Phys. 1994, 189, 99-116.
- (26) Gobrogge, C. A.; Blanchard, H. S.; Walker, R. A. J. Phys. Chem. B **2017**, 121, 4061–4070.

(27) Motlagh, N. S. H.; Parvin, P.; Ghasemi, F.; Atyabi, F. *Biomed. Opt. Express* **2016**, *7*, 2400–2406.

- (28) Karukstis, K. K.; Thompson, E. H. Z.; Whiles, J. A.; Rosenfeld, R. J. Biophys. Chem. 1998, 73, 249–263.
- (29) Lopes, A.; Demelo, J. S.; Martins, A. J.; Macanita, A. L.; Pina, F. S.; Wamhoff, H.; Melo, E. *Environ. Sci. Technol.* **1995**, *29*, 562–570.
- (30) Santos, N. C.; Prieto, M.; Castanho, M. A. Biochim. Biophys. Acta, Biomembr. 2003, 1612, 123-135.
- (31) Olson, F.; Hunt, C.; Szoka, F.; Vail, W.; Papahadjopoulos, D. Biochim. Biophys. Acta, Biomembr. 1979, 557, 9–23.
- (32) Woods, B. L.; George, J. K.; Sherman, A. M.; Callis, P. R.; Walker, R. A. J. Phys. Chem. C **2015**, 119, 14230–14238.
- (33) Chen, J.; Kohler, B. J. Am. Chem. Soc. 2014, 136, 6362-6372.
- (34) Nad, S.; Kumbhakar, M.; Pal, H. J. Phys. Chem. A 2003, 107, 4808-4816.
- (35) Nickels, J. D.; Katsaras, J. In Membrane Hydration: The Role of Water in the Structure and Function of Biological Membranes; Disalvo, E. A., Ed.; Springer: Cham, Switzerland, 2015; pp 45–67, DOI: 10.1007/978-3-319-19060-0 3.
- (36) Tieleman, D. P.; Marrink, S. J.; Berendsen, H. J. C. Biochim. Biophys. Acta, Rev. Biomembr. 1997, 1331, 235-270.
- (37) Swain, J.; Kumar Mishra, A. J. Phys. Chem. B 2015, 119, 12086–12093.
- (38) Sankaram, M.; Easwaran, K. J. Biosci. 1984, 6, 635-642.
- (39) Kučerka, N.; Nieh, M.-P.; Katsaras, J. Biochim. Biophys. Acta, Biomembr. 2011, 1808, 2761-2771.
- (40) Kučerka, N.; Nagle, J. F.; Sachs, J. N.; Feller, S. E.; Pencer, J.; Jackson, A.; Katsaras, J. *Biophys. J.* **2008**, 95, 2356–2367.
- (41) Kwon, J.-H.; Liljestrand, H. M.; Katz, L. E. Environ. Sci. Technol. **2007**, 41, 4011–4018.
- (42) Rogers, J. A.; Davis, S. S. Biochim. Biophys. Acta, Biomembr. 1980, 598, 392-404.
- (43) Evans, E.; Kwok, R. Biochemistry 1982, 21, 4874-4879.
- (44) Ebel, H.; Grabitz, P.; Heimburg, T. J. Phys. Chem. B **2001**, 105, 7353–7360.
- (45) van Wezel, A. P.; Cornelissen, G.; van Miltenburg, J. K.; Opperhuizen, A. *Environ. Toxicol. Chem.* **1996**, *15*, 203–212.
- (46) Wenk, M. R.; Fahr, A.; Reszka, R.; Seelig, J. J. Pharm. Sci. 1996, 85, 228–231.
- (47) Wimley, W. C.; White, S. H. Biochemistry 1993, 32, 6307-6312.